Materials Chemistry and Physics 242 (2020) 122475

Contents lists available at ScienceDirect

Materials Chemistry and Physics

journal homepage: www.elsevier.com/locate/matchemphys

An archaeometallurgical study of Mixtec silver gold alloy foils from Tomb No. 7, Monte Alban, Oaxaca, México

M. Ortega-Avilés [a,*], D. Tenorio-Castilleros [b], I.L. Segura-Venzor [c], José G. Miranda-Hernández [d], M.A. Velasco [e]

[a] Instituto Politécnico Nacional, CNMN, UPALM, Luis Enrique Erro S/N, Zacatenco, C.P. 07738, México CDMX, México
[b] Instituto de Nacional de Investigaciones Nucleares (ININ), Carretera México Toluca-La Marquesa s/n, Ocoyoacac, Estado de México, C.P. 52750, México
[c] Instituto Politécnico Nacional, ESIQIE, UPALM, Av. Instituto Politécnico Nacional s/n, Lindavista, Ciudad de México, C.P. 07738, México
[d] Universidad Autónoma del Estado de México, Centro Universitario UAEM, Valle de México, Boulevard Universitario S/N, Valle Escondido, 54500, San Javier Atizapán de Zaragoza, México
[e] Museo de las Culturas de Oaxaca, Macedonio Alcalá S/N, C.P. 68000, Oaxaca, Oaxaca, México

HIGHLIGHTS

- Silver gold alloy foils belong to Tomb No. 7 from Monte Albán Oaxaca.
- Mixtec goldsmiths prepared Au/Ag/Cu alloys for thin foil fabrication.
- There are solid evidence of depletion gilding to obtain different colorations.
- The microstructure indicates the main mechanical and thermal treatments.
- The nanoindentation is adequate for samples with grain sizes less than 20 μm.

ARTICLE INFO

Keywords:
Monte Albán
Au/Ag/Cu
Microstructure
Indentation hardness (H_{IT})
Indentation modulus (E_{IT})

ABSTRACT

This work evaluates four groups of silver gold alloy foil samples from Tomb No. 7 from Monte Albán, Oaxaca. These were classified as received according to coloration as LG1, LG2, LG3, and LG4. These samples were called silver gold alloy foils because of their main elemental composition. These were analyzed (without alterations) via optical microscopy, scanning electron microscopy (SEM), and energy dispersive spectroscopy (EDS). It was necessary to prepare them by focused ion beam (FIB) cross section to know their real microstructure and finally to test their indentation hardness (H_{IT}) and indentation modulus (E_{IT}) to measure mechanical properties. The experimental results revealed that silver gold alloys were cold-worked and annealed using a mixed technique of hammering with intermediate annealing for grain-size refinement. These were modified in their mechanical properties. The LG2 sample was the thinnest (27 μm) and hardest foil (H_{IT} = 1781.7 MPa). It has the highest Au content (56.9 wt%) and the lowest Cu content (1.5 wt%) unlike LG4, which was the softest foil (H_{IT} = 325.1 MPa). This sample showed non-recrystallized grains: This was the major superficial damage and led to a deficient work metal.

1. Introduction

The Mixtec goldsmiths were the most skilled metalworkers of Mesoamerica: The most important and outstanding collection of gold artifacts of pre-Hispanic Mexico is in the Gold Room of the Museo de las Culturas de Oaxaca. Almost 80% of the existing Mesoamerican gold artifacts belong to the Mixtec Culture [1]. The discovery of Tomb No. 7 from Monte Albán in 1932 by Mr. Alfonso Caso and Valenzuela revealed important data about the Mixtec's funerary customs. This funerary chamber contained the so-called "Treasure of Tomb No. 7 from Monte Albán" with bony remains belonging to several important Mixtec persons and an impressive quantity of objects manufactured with different precious materials such as jade, pearls, turquoise, marine shells, silver, and gold [2,3]. The recovery was highlighted by almost 121 gold pieces

* Corresponding author.
E-mail addresses: maortega@ipn.mx (M. Ortega-Avilés), dtc_nuclear@hotmail.com (D. Tenorio-Castilleros), aneroles17@gmail.com (I.L. Segura-Venzor), jgmirandah@uaemex.mx (J.G. Miranda-Hernández).

https://doi.org/10.1016/j.matchemphys.2019.122475
Received 24 September 2019; Received in revised form 19 November 2019; Accepted 21 November 2019
Available online 25 November 2019

Fig. 1. Gold foils exhibition, Museo de las Culturas de Oaxaca.

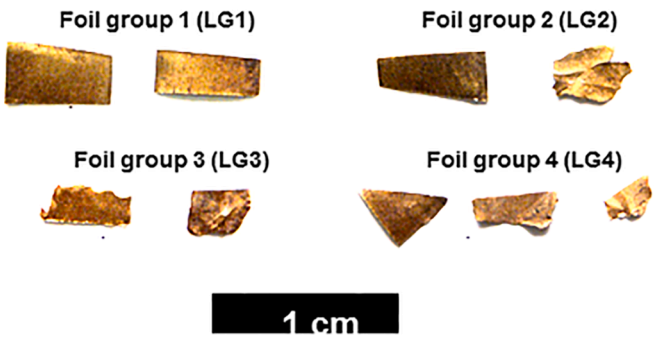

Fig. 2. Classification of silver gold alloy foils, from Tomb No. 7 Monte Albán, Oaxaca.

between breast pieces, rings, false nails, necklaces, bracelets, earrings, a tiara and a feather made of gold foil, broach, and gold foils. There were also objects used as ornamental pieces for funerary rites including corporal ornaments, musical instruments, and tools [2,4,5]. In the late post-Classic period (1300–1521 A.D.), pre-Hispanic goldsmithing in the Oaxaca central valleys developed a proper style and designs that amazed Spanish goldsmiths [3,6]. Monte Albán city was abandoned by the Zapotec culture. It was used later as a necropolis for the Mixtec culture. Funerary customs in ancient Mexico were linked to the huge magic-religious contexts belonging to pre-Hispanic cultures. These are part of daily life according to the cultural groups, social and economic organizations, grade of technological advancements, ideologies, complex religious beliefs, natural resources, and other aspects [7]. Metalwork was concentrated in specific areas of Mesoamerica where different techniques for the manufacture of metal artifacts were adopted and developed [8,9]. Gold and silver metallurgy mainly occurred in the Oaxaca area while copper metallurgy was more common in Western and Central Mexico [1,10,11]. The kind of alloys used in this period were selected according to the desired properties in ornamental wear such as acoustic sound, hardness, coloration, and ductility [2].

Several authors including Motolinia, Las Casas, Sahagún, Bernal, Cortés, and others reported techniques to work with these metals in Mesoamerica. These approaches include ordinary casting, hammering, cold-working, lost-wax casting, false filigree, a mixed technique of hammering with intermediate annealing, and coloration. There were also several types of gilding, ordinary and autogenous welding; wire-drawing, embossed work, metallic covering, and unusual castings [2,4–8,12,13]. Sahagún describes how metal workers used crucibles made with a mixture of vegetal carbon and refractory clay to cast native metals and metals obtained from mineral decomposition (metallic carbonates or sulfates; chapter 16, book IX from the Florentine Codex). These crucibles could also be used to cast several metals together. Thus, such crucibles are rarely found during excavations—they were destroyed after several uses [2,7].

The Mixtec goldsmiths employed several techniques to obtain ingots and artifacts with intricate details for jewelry, pectorals, and bells [12]. The first cold technique used in America was likely hammering for the fabrication of foils with several thicknesses depending on the final use. The technology used in Mixtec goldsmithing to produce gold alloy foils was based on cold-working and intermediate annealing cycles [5]. Cold techniques were applied to native metals and ingots of native metals that had previously been molten. Ethnohistoric sources mention that laminated gold was worked exclusively via hammering to achieve hardness, employing stones with plane characteristics, and stone or copper tools for embossed work [2].

Gold (Au), silver (Ag), and copper (Cu) tend to be ductile and can be mechanically deformed, drawn out into wire, or hammered into sheets [14]. The Au/Ag/Cu alloys are the result of three precious metals combined in a FCC crystalline structure. These show a compact atomic order and are ideal for hammering because of their malleability, toughness, and resistance to brittle fractures. More specifically, gold foils were very useful in Mesoamerica to cover wood and ceramic objects by annealing several times to keep their malleability [2,11,15]. Regarding coloration, the Au/Ag/Cu alloys can vary between reddish, yellowish, and silvery depending on the metals' proportions defined by the metalworkers. These reflect local innovation. Other causes of coloration are changes in the surface composition for several gilding processes such as a depletion process in objects buried for a long time by damaging and corrosive effects, removing metals by etching [2,6], and exposure to heat [13].

Chemical gilding, hand application, and electroplating are modern methods of gilding [13]. Lechtman et al. say depletion gilding was first developed by the Moche culture in Peru from 100 to 800 A.D. This

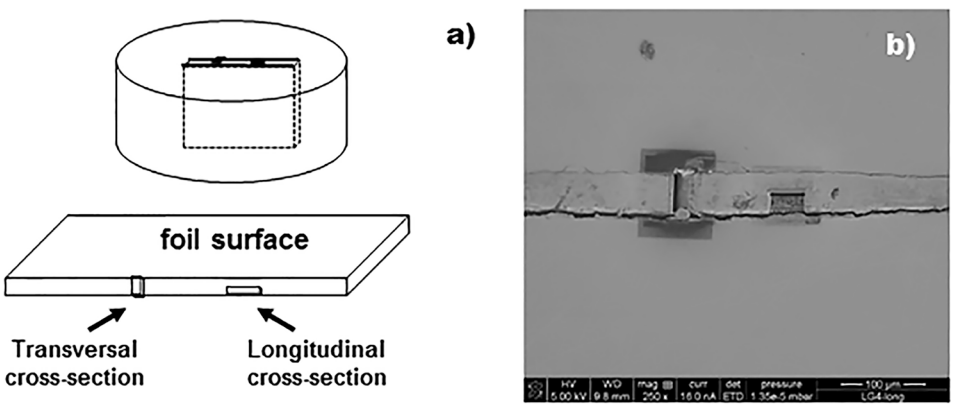

Fig. 3. Sample LG4, a) relative position of silver gold alloy foils mounted in resin, and b) FIB cross-sections, LV-SEM micrograph.

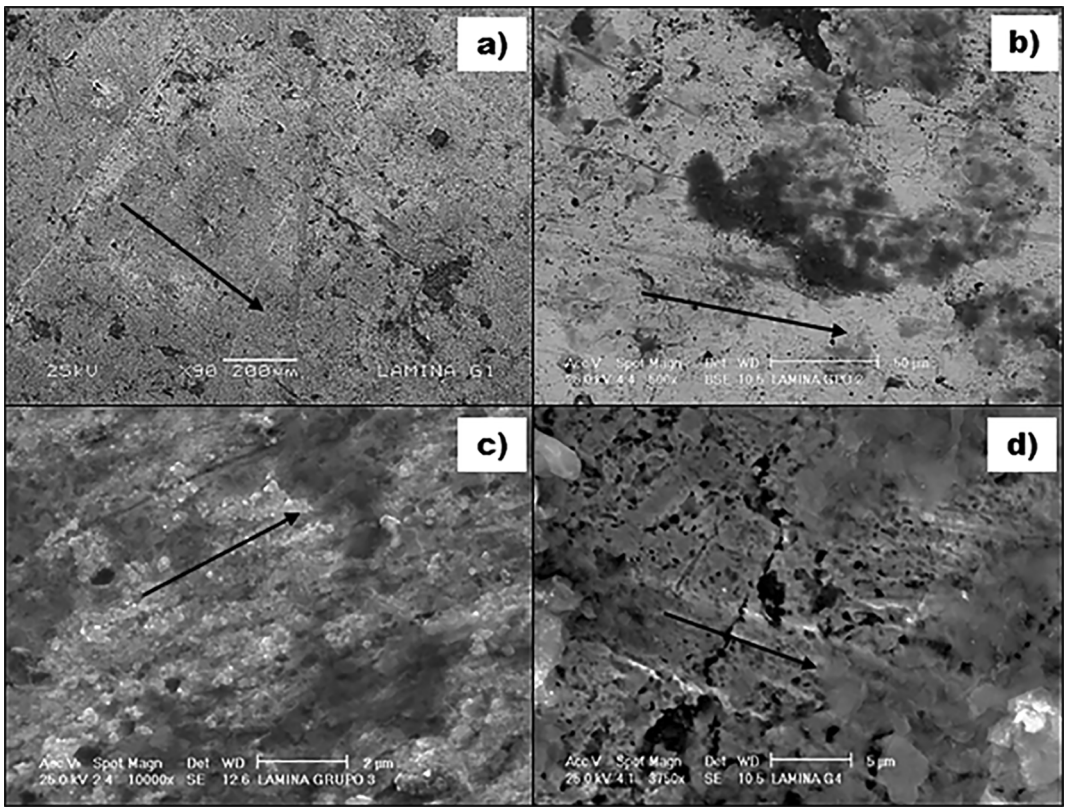

Fig. 4. LV-SEM micrographs of superficial damage in samples as received: a) LG1, b) LG2, c) LG3 and d) LG4.

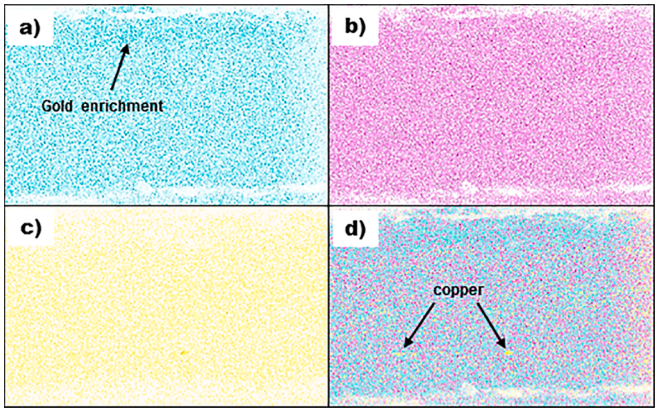

Fig. 5. EDS elemental mapping at 800x: a) Au, b) Ag, c) Cu and d) Composed image. Sample LG1.

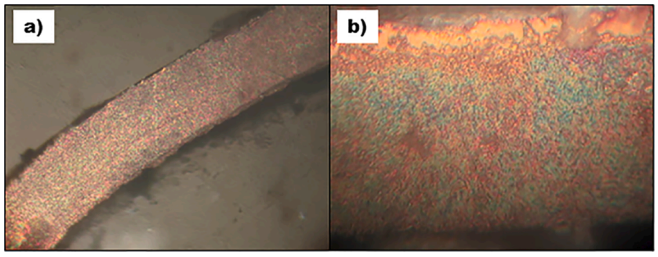

Fig. 6. Metallographic image after chemical etching with *aqua regia* at 600x. Sample LG1.

Table 1
Elemental composition of silver gold alloy foils after FIB cross-section (wt%).

Sample	LG1	LG2	LG3	LG4
Au wt%	25.4	56.9	29.1	25.2
Ag wt%	67.9	41.6	63.6	68.2
Cu wt%	6.7	1.5	7.3	6.6
Total	100%	100%	100%	100%

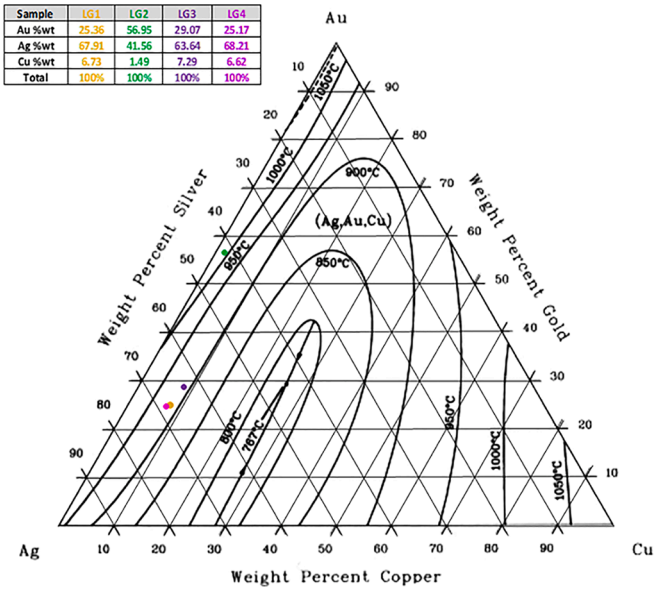

Fig. 7. Liquidus projection of Au/Ag/Cu Ternary Phases Diagram [24].

Table 2
Crystal structure data for the solid binary phases [25].

Solid Phase	(Ag), (Au), (Cu)	α	α1	α2	$AuCu_3$	AuCuI	AuCuII	Au_3Cu
Prototype	Cu	Cu	Cu	Cu	$AuCu_3$	AuCuI	AuCuII	$AuCu_3$

technique then spread into Ecuador, Colombia, Venezuela, Panamá, and Mexico [2,4,9,16]. Most archaeologists believe that the Mesoamerican metallurgy (Mexico and Guatemala) is related to cultures from other regions of Central and South America because of certain similarities: It could have come to the region via maritime trade routes with technologies exploiting a wide range of materials including alloys of Cu/Ag, Cu/As, Cu/Sn, and Cu/As/Sn [4,6,8,11,17]. IN today's society, gold is used in money, jewelry, decoration, dental work, plating, and a wide range of electrical circuit applications [11].

There are few studies on the gold alloy objects from Tomb 7 at Monte Albán using microchemical tests, SEM, EDS, and nondestructive techniques such as proton-induced X-ray emission (PIXE), X-Ray fluorescence (XRF), and UV/Vis spectroscopy (UV–Vis) [2,3,5,9,11]. Modern nanoindentation studies of gold and gold alloys can determine nanoindentation hardness and stacking fault energies via classical molecular simulations [18]. The results can correlate hardness and onset of plasticity of single crystalline gold thin films to understand their mechanical properties [19]. However, this has not been extended to the analysis of cultural patrimony objects. Our goals was to extend this analysis to the objects from Tomb No. 7 of Monte Albán, Oaxaca to learn about the techniques and manufacturing processes involved in their production.

The foil samples were initially analyzed as received via optical microscopy, SEM, and EDS. Next, the samples were mounted in cross section using a resin and etched to reveal microstructure. We prepared the samples by a FIB cross section to reveal the real microstructure, alloy composition, and internal porosity. Finally, tests for indentation hardness (H_{IT}) and indentation modulus (E_{IT}) were performed.

2. Materials and methods

2.1. Archaeological material

The Gold Room of the Museo de las Culturas de Oaxaca exhibits famous gold pieces from the most important collection of gold artifacts in Mexico [1] including breast pieces, pendants, bracelets, rings, necklaces, chin ornaments, zoomorphic pieces, bells, and big gold foils (Fig. 1).

Small fragments of silver gold alloy foils were collected from a small box with pieces of several materials from Tomb No. 7; this box remained in the museum collection. The small fragments of silver gold foils were studied as received without cleaning or alteration, and before to known their chemical compositions. They were classified in four groups according to their superficial color and labelled as LG1, LG2, LG3, and LG4 (Fig. 2).

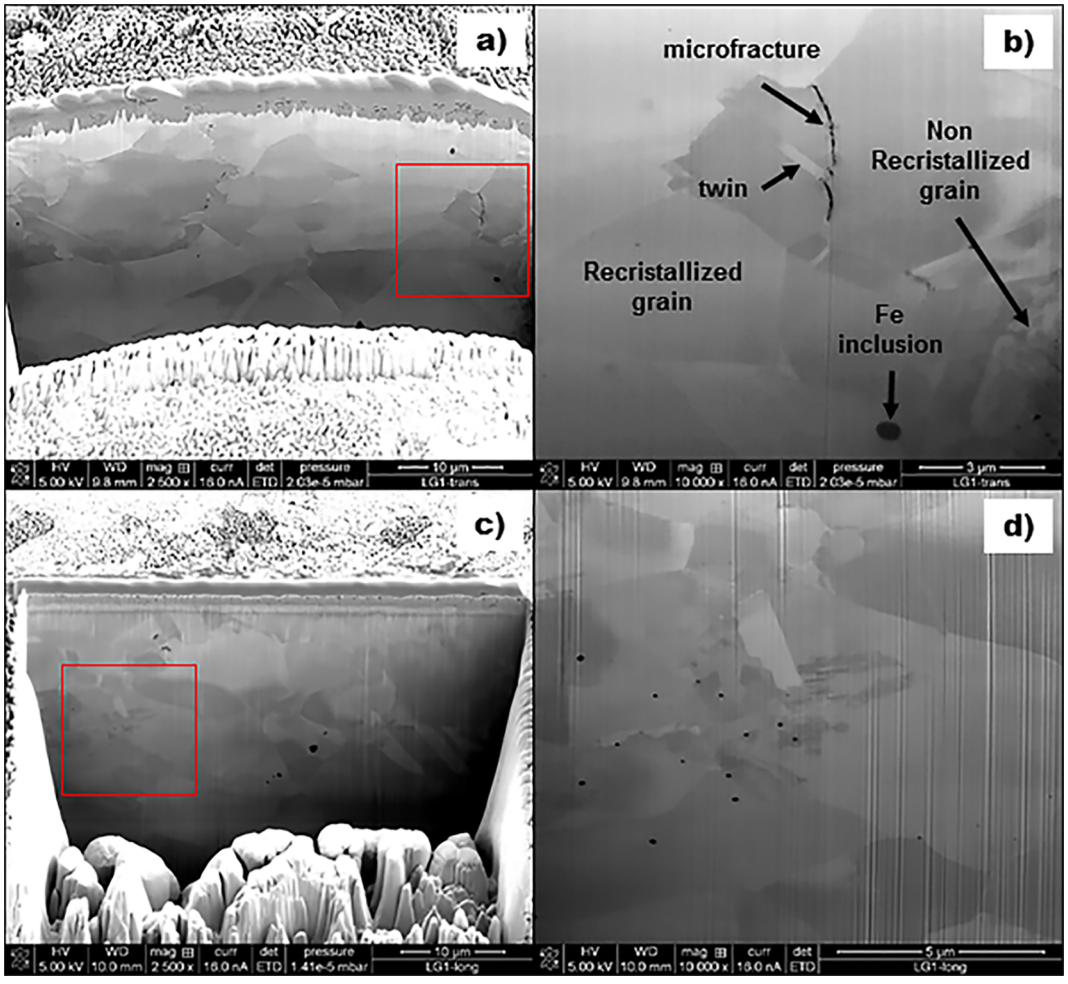

Fig. 8. FIB cross-section showing microstructure of sample LG1, a,b) transversal section and c,d) longitudinal section.

2.2. Techniques

The first examination was low vacuum scanning electron microscopy (LV-SEM) using an SEM model FEI XL-30 to observe the surface details without chemical etching or any metallographic preparation. The first approach for elemental composition and superficial mapping used EDS. One piece of each group was selected, and a small section (4 × 2 mm) was cut with sharp tweezers while trying to avoid deformation. The sample was mounted in transversal sections using resin with a circular mold 1 cm in diameter (Fig. 3a). The entire sample was polished and etched to reveal their microstructures while applying ASTM E−93 and ASTM E−407-93 standards [20]; optical photographs were recorded. A Dual Beam Quanta 3D FEG from FEI Co. was used to make two erosions with FIB via gallium ions: One was in a transverse cross section, and the other was a longitudinal cross section (Fig. 3b). It is difficult to cross-section particles and mechanically-weak structures. It is also difficult to generate smear-free cross-sections of structures having layers of differing hardnesses; however, this becomes routine with the dual beam FIB. It is a tool for cross-sectioning MEMS devices without inducing catastrophic damage. This tool can produce artifact-free cross-sections of almost any material [21].

The samples were analyzed with SEM and EDS again after the erosion of the two cross sections to identify the real microstructure and elemental composition. Finally, the load P and the displacement h were measured continuously during the test in the nanoindentation technique. This approach could extract the elastic modulus known as indentation modulus (E_{IT}) and hardness called indentation hardness (H_{IT}) of the material from load-displacement measurements [22,23] with a CSM Instrument model TTX-NHT-bERCOVICH with a Berkovich indenter and a force of 5 μN. Seven indentation tests were realized in each sample, and all data are mean curves from the five best tests.

3. Results and discussion

3.1. Superficial LV-SEM analysis (superficial damage, porosity and EDS on the samples as received)

A superficial inspection of each silver gold alloy foil sample was performed as received via LV-SEM to observe superficial damage caused by processing, corrosion processes during burial, and ancient sample management. LG1 samples had superficial damage such as pitting due to copper loss during the possible gilding process or due to environmental corrosion effects after hundreds of years at the burial site. Damage marks are 20–180 μm (Fig. 4a). These holes usually contain some materials such as powders. Topographic heterogeneities such as superficial protrudes and pores with several sizes are seen. EDS showed 61.2 wt% Au, 20.6 wt% Ag, and 1.4 wt% Cu, which represents almost 83.2 wt%. The most common nonmetallic elements were C, O, Al, and Si representing about 15.0 wt%. Trace levels of Na, Mg, K, Ca, and Fe constitute the remaining 1.9 wt%. A relevant detail was the presence of micro-inclusions with iron. This led to additional non-metallic micro-inclusions due to the nature of the manufacturing process and direct contact with the burial ground.

The LG2 samples had superficial damage such as pitting and porosity (Fig. 4b). They had the same kind of superficial damage and nonmetallic micro-inclusions. The superficial EDS results showed that the content of Au, Ag, and Cu were 51.7 wt %, 13.0 wt%, and 0.9 wt%, respectively. This group had Zr in very small as agglomerations.

In the LG3 group, different superficial damages were present than in the other groups of gold foils. They had superficial small rounded particles on the order of 200 nm in diameter. These were mainly seen in the big areas (Fig. 4c); LV-SEM micrographs showed topographic heterogeneities, longitudinal marks, and pores. Regarding the foils' elemental compositions, the first approach on the received samples by EDS showed

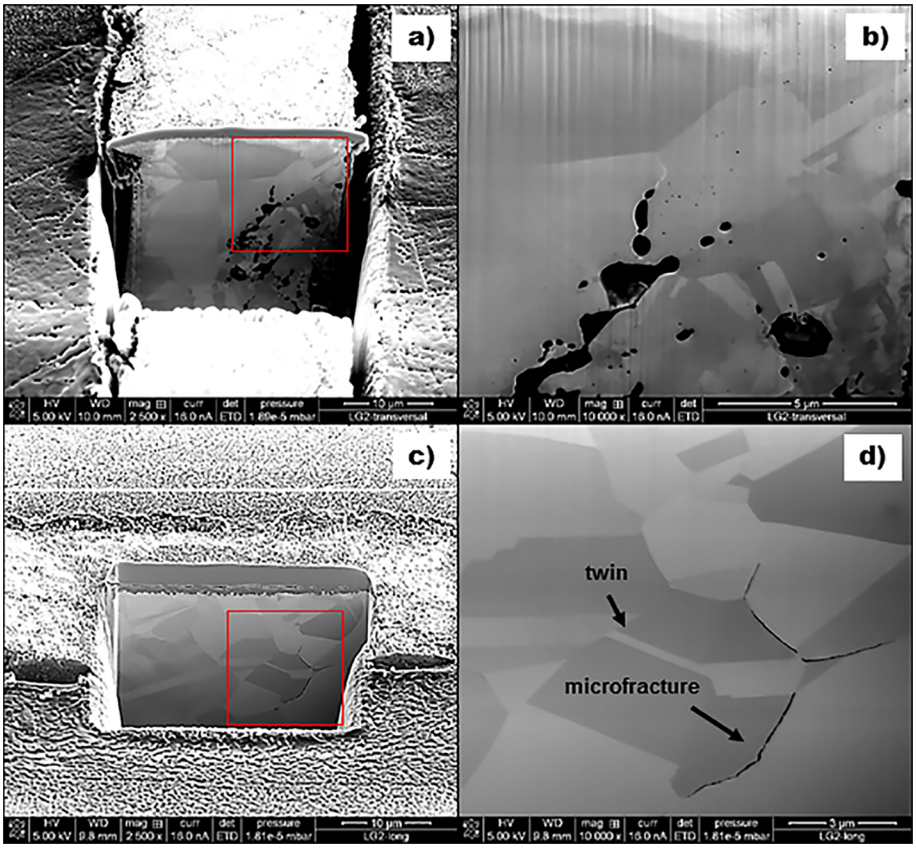

Fig. 9. FIB cross-section showing microstructure of sample LG2, a,b) transversal section and c,d) longitudinal section.

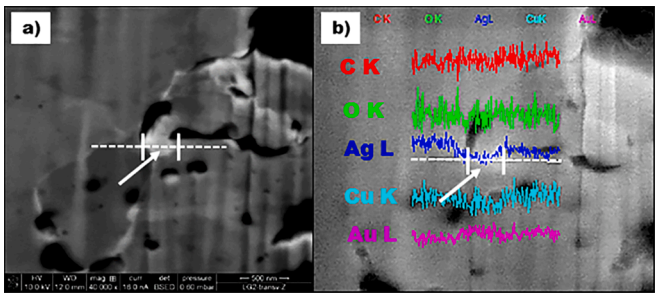

Fig. 10. EBSD micrograph and X-ray line scans on transversal section. Sample LG2.

the main elemental composition as 42.1 wt% Au, 36.2 wt% Ag, and 6.9 wt% Cu, which represents almost 85.2 wt%. The nonmetallic elements identified in this group of foils were C, O, and Si representing approximately 14.8 wt%. Nonmetallic micro-inclusions were identified in the LG1 sample.

The last LG4 group had the major superficial damage and extensive areas with big pores that appear interconnected. They create narrow channels similar to furrows (Fig. 4d); this may be a result of intensive gilding processes or exposure to environmental corrosion effects. In addition, superficial EDS results showed Au, Ag, and Cu amounts of 32.1 wt%, 16.1 wt%, and 1.2 wt%, respectively. The iron presence in this sample was remarkable (2 wt%) and probably came from the vessel or tools used for the foil processing. The remaining elements were C, O, Mg, Al, Si, and Ca. There were many materials sucked in the surface and incrusted in the pores— feldspars, clays, quartz, and some minerals from the burial site.

The corrosion damage in the samples was probably related to the removal of Cu from the surface and corrosion processes during burial. LV-SEM observations at 100x of the samples helped us establish a proper order of superficial porosity as follows: LG4 > LG3 > LG1 > LG2. Moreover, according to the first EDS approach, the samples richest in Au showed minor porosity because this metal dominates the properties of the alloy, which is less prone to corrosion than Cu. The LG2 sample had the highest Au content followed by LG1, LG4, and LG3. LG3 had the highest amount of Ag followed by LG4, LG1, and LG2. LG3 had the most Cu followed by LG4, LG1, and LG2.

3.2. *Thickness, elemental mapping, and chemical etching*

The thickness foils were less than 1 mm. They are on the order of microns and were 60 μm, 27 μm, 61 μm, and 48 μm for LG1, LG2, LG3, and LG4, respectively. Fig. 5 shows the elemental maps of precious metals in sample LG1 mounted in resin at 800x where the lateral sides are located on the top and bottom of each image and correspond to the original surfaces of the silver gold alloy foil. The elemental distribution of Au (Fig. 5a), Ag (Fig. 5b), and Cu (Fig. 5c) appear uniformly distributed. However, upon observing the composed image with overlapping maps, one can see certain gold enrichment on the top and small concentrations of copper in areas slightly bigger than the gold and silver in the center of the foil (Fig. 5d). The elemental maps on the four samples indicate that Au, Ag, and Cu distributions are not completely

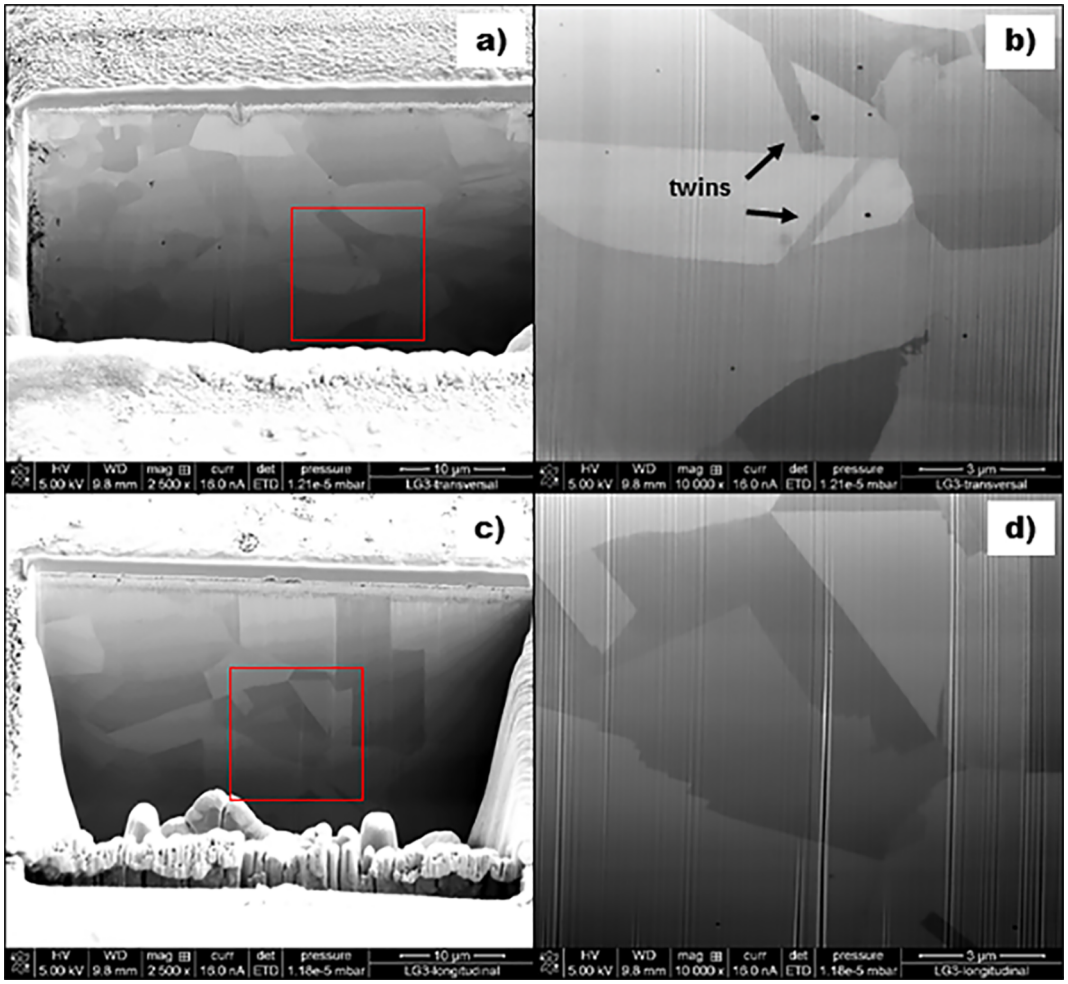

Fig. 11. FIB cross-section showing microstructure of sample LG3, a,b) transversal section and c,d) longitudinal section.

homogeneous in the transversal section before chemical etching with *aqua regia* to reveal their microstructure. After chemical etching, samples mounted in the transverse section do not present defined grain boundaries at 600x magnification. This suggests that the grain size could be extremely small; it is even possible to appreciate three different colors: green, purple, and red corresponding to copper, silver, and gold, respectively (Fig. 6a). Reddish coloration in the edge of the sample indicates gold enrichment on the foil surface (Fig. 6b).

3.3. Elemental composition by EDS after FIB cross-sections and phase diagram

EDS analyses was repeated after FIB cross sectioning of an undamaged surface without traces of the abrasives used for polishing. We compared the wt% contents of the precious metals. LG1, LG3, and LG4 have similar compositions with 25.2–29.1 wt% Au, 63.6–68.2 wt% Ag, and 6.6–7.3 wt% Cu. These results could indicate that Mixtec goldsmiths prepared Au/Ag/Cu alloys with similar elemental compositions for foil elaboration. These are closer to actual 6-karat and 7-karat alloys. In contrast, LG2 had different contents of these metals. It had the highest Au content (56.9 wt%) and the lowest Cu content (1.5 wt%) with 41.6 wt % of Ag close to actual 14-karat alloyat 58.5 wt% (Table 1). A comparison between the first EDS approaches of the received samples is different to the EDS analysis over the cross section surface—especially in Cu content that is higher in the cross section (nucleus of the foil) than in the surface without cleaning. This suggests copper loss from the applied gilding processes. Most ancient metals are impure or are deliberate alloys of two or more metals. Native gold usually contains some copper and silver; typical gold concentrations are 85–95 wt% with the remainder being mostly silver [14]. Table 1 demonstrates that these Au/Ag/Cu alloys are different than native gold and purpose fully prepared.

Fig. 7 presents the liquidus diagram for the Au/Ag/Cu system including the points corresponding to LG1, LG2, LG3, and LG4 compositions (wt%) [24]. The LG1 and LG4 present almost the same composition, and the LG3 composition is close to the elemental composition. The LG2 sample has the highest Au (56.9 wt%) and Ag (41.6 wt%) content with the lowest Cu content (1.5 wt%). Fig. 7 shows that LG1, LG3, and LG4 were processed at almost the same temperature, which is close to the melting point of Ag ($T_{Ag} = 961.8\ ^{\circ}C$). LG2 was processed at the highest temperature—less than the melting points of Au and Cu ($T_{Au} = 1064\ ^{\circ}C$; $T_{Cu} = 1085\ ^{\circ}C$). Materials made from this system have a wide range of flow points due to the wide temperature range covered by the liquidus surface [20]. The most important colored alloy systems with gold bases are Au/Ag/Cu alloys. They maintain 18-karat or 14-karat specifications and can result in a yellow, pink, or red color by varying the concentration of silver and copper [25].

Comparing our results for silver gold alloy foils from Tomb No. 7 with others reported by Peñuelas et al., the compositions are different than those reported for artifacts belonging to different museum collections: MNAH Museo Nacional de Antropología e Historia (Zaachila-Oaxaca, Aztecs, Maya), MTM Museo del Templo Mayor (Aztecs), MCO Museo de las Culturas de Oaxaca (Tomb 7 Monte Albán, Caxonos), and BSV Baluarte de Santiago Veracruz (Fisherman's Treasure). The analyzed pieces by Peñuelas et al. from Tomb No. 7 were compared with other gold collections from Oaxaca and other Mesoamerican areas.

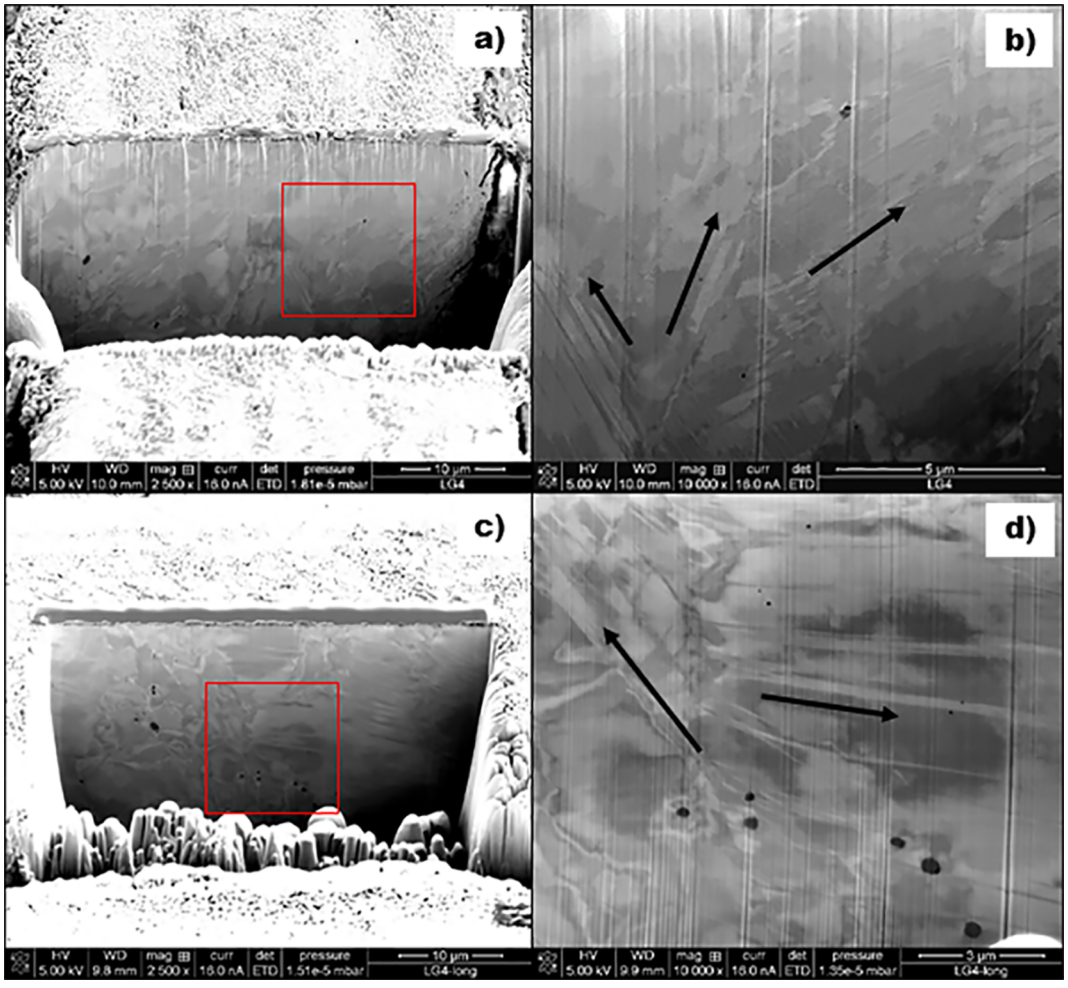

Fig. 12. FIB cross-section showing microstructure of sample LG4, a,b) transversal section and c,d) longitudinal section.

Table 3
Composition, physical and mechanical characteristics of foil samples.

Sample	Thickness(μm)	Range Grain size (μm)	Pores Average size(nm)	Au wt%	Ag wt%	Cu wt%	H_{IT} (MPa)	E_{IT} (GPa)
LG1	60	1–12	57	25.4	67.9	6.7	689.13	36.57
LG2	27	0.6–12	148	56.9	41.6	1.5	1781.70	51.93
LG3	61	1–14	137	29.1	63.6	7.3	1091.89	32.5
LG4	48	ND	106	25.2	68.2	6.6	325.13	17.1

ND – not determined.

There was good agreement with the composition of objects from the Central Valleys of Oaxaca and Aztec. The gold in the Aztec area likely came from Oaxaca—this gold was obtained as powder, flakes, and nuggets from secondary deposits or on the banks of the rivers [4]. However, artifacts from Tomb No. 7 have a different composition to Maya, Caxonos, and Fisherman's Treasure items. The Ag alloys from Tomb No. 7 had less than 5 wt% of Au and Ag contents higher than 90 wt % [3]. In this sense, they are best described as silver/gold alloy foils because the Ag content is 41 wt % - 68 wt%, and the Au content is in the order of 25 wt% - 57 wt%. We next compared the composition of these foil samples with the ternary diagram Au/Ag/Cu reported by Peñuelas. Three silver gold alloy samples are in the gap of the phase diagram between 20 wt% Au and 50 wt% Au with no known museum artifacts of this type [3]. Carmona mentioned that the Mixtec goldsmiths preferred to alloy gold with silver to reduce the temperature during casting and attain high-quality objects [4].

Currently, no ternary compounds have been reported in the Au/Ag/Cu ternary system [25]; three main features enter into the ternary equilibrium diagram: the AuCu and Cu_3Au superlattices as well as the region of separation in two FCC phases (solid solution region) that arise in the Ag/Cu system [26]. Table 2 summarizes the crystal structure data for the binary phases of the Au/Ag/Cu system.

The three binary subsystems, Au/Cu, Ag/Au, and Ag/Cu behave quite differently [27]. The classical ordering system Au/Cu forms three different ordered phases: All of the FCC type are $AuCu_3$, AuCu, and Au_3Cu. The Ag/Au forms a solid solution over the entire composition range in the liquid and solid states [24]. The Ag/Cu decomposes into a Cu-rich and Ag-rich FCC phase. The ternary system Au/Ag/Cu is dominated by the miscibility gap coming from the Ag/Cu binary edge and the amount of Ag that dissolves in the ordered Au/Cu phases [27]. Upon addition of Ag, the ordered phases that exist below 410 °C on the solidus diagram in the Au/Cu binary system are rapidly suppressed and soon disappear [24]. Experimental information published for the Au/Ag/Cu system from different authors is inconsistent; there is a discrepancy between calculated and experimental phase diagrams [24–27]. These data, combined with the fact that diagrams usually only refer to very slowly cooled metals that rarely occur in archaeological materials [14], make it difficult to predict with accuracy what phases should be present in the gold alloy foils and the heat treatment temperatures.

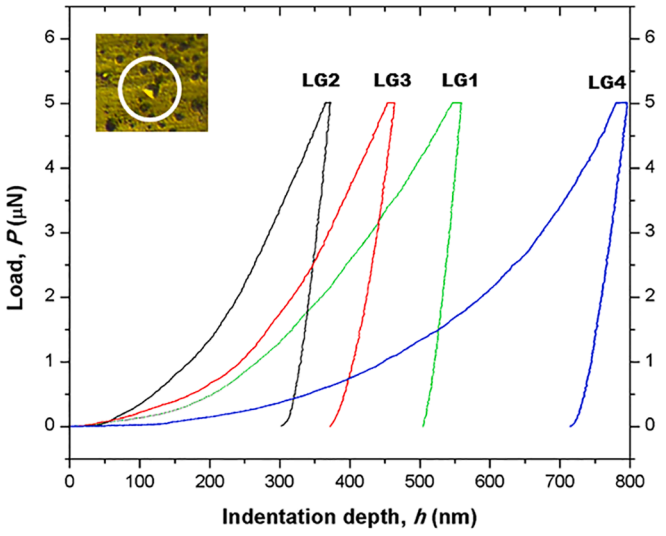

Fig. 13. Load-displacement curves from Nanoindentation tests with Berkovich indenter.

3.4. Microstructure and internal porosity in FIB cross-sections

To reveal the thin foil microstructures, a FIB cross-section with a polished finish was carried out in two relative positions as described in Fig. 3: transversal and longitudinal sections. Four micrographs were presented for each sample. Two are a transversal section at 2,500x and 10,000x, and two are a longitudinal section at the same magnifications to reveal micrometric and nanometric details. The LG1 sample in transversal section shows mainly recrystallized grains together with small areas with no recrystallized grains (Fig. 8a) or annealing twins. There are some intergranular micro fractures with a length of about 4 μm and tiny iron inclusions (Fig. 8b); moreover, the grain size is in the range of 1–12 μm. In Fig. 9c and d, degasification pores appear with different sizes: macropores bigger than 50 nm (from 54 to 68 nm) and mesopores smaller than 50 nm (44 nm) are far away from the edges of the foil.

Sample LG2 is the thinnest foil and only has grains completely recrystallized and annealed in twins. It has macropores from 71 to 560 nm and mesopores from 16 to 47 nm. The big pores in the right side of the transversal section images were probably produced during corrosion process during burial (Fig. 9a and b).

The longitudinal section does not have any pores—only some intergranular microfractures close to the surface of the foil with lengths of 1–4 μm and twinned equiaxed grains with sizes between 0.6 and 12 μm (Fig. 9c and d). Some Fe inclusions in the range from 600 to 1000 nm were identified. The EBSD image of the LG2 sample shows areas with different compositions in Fig. 10a; high Z-contrast is especially common at grain boundaries. The brightest area is 500 nm on diameter and was selected to obtain elemental profiles of Au, Ag, and Cu. In Fig. 10b, the X-ray line scans of Au, Ag, and Cu indicate the elemental variation along the white outline; the white arrow points to the line section where the Ag and Cu signals decrease and the Au signal increases. This is evidence of a probable second phase rich in Au different to the equiaxial grains of uniform composition.

The LG3 sample has equiaxial grains of 1–14 μm with some annealing twins (Fig. 11a–d) as well as macropores with sizes of 73–326 nm. Intergranular micro fractures were not observed, but inclusions from 200 to 1000 nm containing Fe were identified. LG4 had macropores with sizes from 52 to 343 nm, and some mesopores smaller than 50 nm were observed in longitudinal and transversal sections as in the LG3 foil sample. The most important characteristic in the microstructure of this sample was the domain of non-recrystallized grains in both sections (Fig. 12). Clearly, there are no signals of grain enlargement in the deformation direction as the black arrows highlight (Fig. 12b and d). Small iron inclusions (300–1000 nm) were also identified as in the LG1 sample.

LV-SEM micrographs indicate that the original cast Au/Ag/Cu alloys were cold worked and annealed using a mixed technique of hammering

with intermediate annealing [7]. The microstructure revealed the main mechanical and thermal treatments established for the metal [28,31]. FCC metals except for aluminum recrystallize by a twinning process [14]. The processes that occur during annealing of metals are recovery, recrystallization, and grain growth [15,30]. In cold-working, strain hardening occurs due to plastic deformation below the recrystallization temperature. Recrystallization will occur in a reasonable time (e.g., 1 h) when the temperature is between 0.3 and 0.6 of the absolute melting point. Moreover, this recrystallization temperature is affected by different factors such as the chemical composition of the alloy, the amount and type of plastic deformation, the time for the annealing temperature, the original grain size, and the deformation temperature [31].

The LG1, LG2, and LG3 samples showed well-developed equiaxial grains and annealing twins due to operation at proper temperatures and times. The LG4 was probably cooled very rapidly, and the normal crystalline structure was suppressed. Slowly cooled melts rarely occur in archaeological materials [14]. On the other hand, the Au/Ag/Cu alloys have low vapor pressure, and therefore there is negligible volatilization at their normal casting temperatures at approximately 1200 °C [32]. Usually, liquid metals contain certain amounts of dissolved gases; they are removed when the annealing temperature decreases [7]. The micro porosity occurs during solidification process. The presence of pores in MesoAmerican objects is due to the high temperatures up to the alloys' melting points (it is known that Mixtec goldsmiths were capable of reaching high temperatures). The micro porosity has been reported for cast metals with pore sizes from 5 to 0 μm in columnar grains and 25 μm for equiaxial grains [15]. Nevertheless, in the case of these samples, the degasification pore sizes are in the range of 57–147 nm after several cold-worked annealing cycles. Finally, the presence of intergranular micro fractures in LG1 and LG2 indicate that these foils were fractured after a certain amount of plastic deformation at low temperatures [7,14]. Data about grain and pore average sizes are presented in Table 3.

3.5. Indentation hardness (H_{IT}) and indentation modulus (E_{IT})

Experimental deep penetration versus load curves (Fig. 13) show a hold period at a maximum load of 5 μN in a typical test cycle. The LG2 sample was 27.3 μm thick and is the hardest (H_{IT} = 1781.70 MPa/E_{IT} = 51.93 GPa). LG4 was 48.33 μm thick and is the softest (H_{IT} = 325.13 MPa/E_{IT} = 17.1 GPa). Samples LG1 and LG3 had values of 689.13 MPa/E_{IT} = 36.57 GPa and 1091.89 MPa/E_{IT} = 32.5 GPa, respectively. They had almost the same thickness foil (60 and 61.02 μm) and can be observed in Table 3.

In general, samples LG1, LG3, and LG4 have similar chemical compositions and thicknesses. They have similar H_{IT} values; nevertheless, the difference in H_{IT} values can be attributed to their microstructures as a result of annealing temperatures and time applied during the final thermal treating.

Gold with a purity of 99.90–99.99% has a unique property among metals: its oxide is unstable (its surface remains bright indefinitely) [29]. It is also extremely soft and ductile. It is known that the hardness increases with trace impurities and rapidly rises with cold-work. The effect on the hardness and ductility of the Au/Ag/Cu alloy depends on the proportions of Ag and Cu. Moreover, the rate of hardening on cold-working increases much faster with Cu than with Ag. In the cold-worked material, the final ductility on the hard-drawn alloy increases with the Ag content [32]. The traditional methods of strengthening include work hardening, formation of solid solutions, precipitation hardening, and grain-size refinement [18,31]; the mechanical properties of solid solutions are sensitive to grain size in the sense that the hardness and strength increase for Au/Ag/Cu alloys as the grain size is reduced [15].

The grain size in traditional polycrystalline metals is on the order of 25–150 μm [15]. In this case and for Au/Ag/Cu foils, the grain size is 0.6–14 μm as a result of cold-working and annealing cycles, which explains their mechanical properties. Many improved strengths of different karat golds have been developed, and H_V hardness values for annealing and cold-work include 18-karat gold (Au 75 wt%; Ag 12.5 wt %; Cu 12.5 wt%) with annealed hardness Hv values of 110 [32] and 150 [33]; the cold-worked hardness Hv was 190–225 [33]. Relatively few micro-hardness values have been reported for ancient gold alloys. In the case of a nail and a foil with the same composition (Au 83.7 wt%, Ag 12.8 wt%, Cu 1.5 wt%, Fe, Pt, Sb, Ni, As, Pb, and Si), the highest Hv value of 60 was obtained from the nail tip, and the Hv values from the gold foil were 37 and 49 [14]. Nanoindentation tests are more adequate for archaeometric studies in small samples with grain sizes less than 20 μm because they provide the hardness of individual phases or grains in the sample. The indentation marks are in the range of 50–100 nm, and the damage is almost imperceptible unlike the Brinell and Vickers indenter marks used for micro-indentation tests.

4. Conclusions

Mixtec goldsmiths used Au/Ag/Cu alloys for thin foil fabrication. All samples analyzed contain these three elements in different proportions with compositions close to modern 6-karat, 7-karat, and 14-karat gold. Samples LG1, LG3, and LG4 have almost the same composition in wt%. These may have been deliberately specified for silver gold alloy foil elaboration. Superficial damage observations by LV-SEM and EDS mapping in cross section before chemical etching are solid evidence of depletion gilding processes applied to obtain different colorations by removing copper or producing corrosion process during burial. Microstructure identification via metallographic analysis was not possible. Thus, FIB erosion was necessary to reveal the microstructural details at the micrometric and nanometric levels. This metallurgical insight is not visible using traditional metallographic observations. LV-SEM micrographs revealed that original casting Au/Ag/Cu alloys were cold-worked and annealed using a mixed technique of hammering with intermediate annealing for grain-size refinement. These were modified in their mechanical properties. The LG2 sample was the thinnest and hardest foil. It had the highest Au content and the lowest Cu content unlike LG4 that has the softest foil with non-recrystallized grains. The major superficial damage was present on the as-received sample and suggests deficient work metal. Moreover, the LG4 sample presented intermediate values of thickness and Au content as well as the highest Cu content. Samples LG1 and LG3 were the thicker foils with similar ranges of grain size and Au, Ag, and Cu contents but different indentation hardness and indentation modulus values. This is probably due to LG1 having small areas with no recrystallized grains as shown in LV-SEM micrographs. The experimental results indicate that Mixtec goldsmiths sometimes did not have precise control of all variables during metalworking.

Acknowledgements

We acknowledge to Consejo de Arqueología (INAH), for the permission to study these materials, and Roberto Carlos González Díaz and Miguel Ernesto Gachuz Méndez for their support in laboratory and valuable advices. This research did not receive any specific grant from founding agencies in the public, commercial, or not-for-profit sectors.

References

[1] J.L. Ruvalcaba Sil, G. Peñuelas Guerrero, J. Contreras Vargas, E. Ortíz Díaz, E. Hernández Vázquez, Technological and material features of the gold work of Mesoamerica, ArchaeoScience Revue d'archéometrie 33 (2009) 289–297, https://doi.org/10.4000/archeosciences.2345.

[2] A. Caso, El Tesoro de Monte Albán (Memorias del INAH III, INAH – SEP, México, 1969.

[3] G. Peñuelas, J.L. Ruvalcaba, J. Contreras, E. Hernández, E. Ortíz, Non-destructive in situ analysis of gold and silver artifacts from Tomb 7 Monte Albán, Oaxaca, México, in: Proceedings of the 37th International Symposium on Archaeometry, Siena Italy, 2008, https://doi.org/10.1007/978-3-642-14678-7_91.

[4] M. Carmona Macías, Entre Crisoles y Dioses: La Orfebrería Prehispánica de Oaxaca, Historia del Arte de Oaxaca, Arte Prehispánico Vol. I, Gobierno del Estado de Oaxaca, Instituto Oaxaqueño de las Culturas, México, 1997.
[5] G.A. Camacho-Bragado, M. Ortega-Avilés, M.A. Velasco, M. José Yacamán, A microstructural study of gold treasure from Monte Alban's Tomb 7, J. Occup. Med. 57 (7) (2005) 19–24. https://doi.org/10.1007/s11837-005-0247-2.
[6] Salvador Toscano, Arte Precolombino de México y de la América Central, Instituto de Investigaciones Estéticas, UNAM, México, 1994.
[7] D.M.K. de Grinberg, Los Señores del Metal: Minería y Metalurgia en Mesoamérica, Consejo Pangea Editores S.A. de C.V., México, 1991.
[8] F. Franco, A. Macías, in: Eduardo Williams (Ed.), Análisis de los Metales Prehispánicos Tarascos de Huandacareo, Michoacán, Contribuciones a la Arqueología y Etnohistoria del Occidente de México, Colegio de Michoacán, México, 1994.
[9] G. Demortier, J.L. Ruvalcaba-Sil, Differential PIXE analysis of mesoamerican jewelry items, Nucl. Instrum. Methods Phys. Res. B 118 (1996) 352–358, https://doi.org/10.1016/0168-583X(96)00248-0.
[10] E. Ortíz Díaz, Location of gold placers in Oaxaca, ArchaeoScience Revue d'Archéometrie 33 (2009) 303–307, https://doi.org/10.4000/archeosciences.2365.
[11] D.M.K. de Grinberg, Crisol de Técnicas, Metalurgia del México Antigüo, Arqueol. Mex. 19 (1996) 4–11.
[12] D. Hosler, The Sounds and Colors of Power, the Sacred Metallurgical Technology of Ancient West México, The MIT Press, Cambridge, Massachusetss, London, England, 1994, ISBN 9780262082303.
[13] A.C. Sparavigna, Depletion gilding: an ancient method for surface enrichment of gold alloys, Mechanics, Mat. Sci. Eng. (2016), https://doi.org/10.13140/RG.2.1.2329.4485.
[14] D.A. Scott, Metallography and Microstructure of Ancient and Historical Metals, Getty Conservation Institute, The G. Paul Getty Museum in association with Archetype Books, 1991, ISBN 0-89236-195-6.
[15] J.D. Verhoeven, in: Limusa (Ed.), Fundamentos de Metalurgia Física, 1987, ISBN 0-471-90616-6. México.
[16] H. Lechtman, A. Erlij, E.G. Barry Jr., New perspectives on Moche metallurgy: techniques of gilding copper at loma Negra, Northern perú, Am. Antiq. 47 (1) (1982) 3–30. https://doi.org/10.2307/280051, 10.2307/280051.
[17] L. Vetter, P. Carcedo, S. Cutipa, E. Montoya, Estudio Descriptivo, Metalográfico y Químico de las Puntas de Aleación Cobre de la Tumba de un Señor de la élite Sicán, Lambayeque – perú, empleando técnicas de microscopía óptica y análisis por activación neutrónica, Rev. Española Antropol. Am. 27 (1997) 23–38. Servicio de Publicaciones Universidad Complutense, Madrid.
[18] L. Yangzhong, A. Goyal, A. Chernatynskiy, J.S. Jayashankar, M.C. Kautzky, S. B. Sinnott, R. Simon Phillpot, Nanoindentation of gold and gold alloys by molecular dynamics simulation, Mater. Sci. Eng. A 651 (2016) 346–357, https://doi.org/10.1016/j.msea.2015.10.081.
[19] M. Dietiker, R.D. Nyilas, C. Solenthaler, R. Spolenak, Nanoindentation of single-crystalline gold thin films: correlating hardness and the onset of plasticity, Acta Mater. 56 (2008) 3887–3899, https://doi.org/10.1016/j.actamat.2008.04.032.
[20] V. Voort, F. George, ASM Handbook, Volume 09 - Metallography and Microstructures, ASM International, 2004. https://app.knovel.com/hotlink/toc/id:kpASMHVMM1/asm-handbook-volume-09/asm-handbook-volume-09. accesed june 2018.
[21] L.A. Giannuzzi, B.I. Prenitzer, B.W. Kempshall, M.W. Phaneuf, in: Lucille A. Giannuzzi, Fred A. Stevie (Eds.), Introduction to Focused Ion Beams, Instrumentation, Theory, Techniques and Practice, Springer, Boston, 2005, ISBN 0-387-23116-1. Print.
[22] G. Guillonneau, Determination of mechanical properties by nanoindentation independently of indentation depth measurement, J. Mater. Res. 27 (19) (2012) 2551–2560, https://doi.org/10.1557/jmr.2012.261.
[23] A.C. Fischer-Cripps, Nanoindentation, Mechanical Engineering Series, 2011, ISBN 978-1-4419-9872-9.
[24] Alloy Phase Diagrams, ASM Handbook, vol 3, The Materials Information Society, 2005.
[25] A. Prince, G.V. Raynor, D.S. Evans, in: London, V.T. Brookfield (Eds.), Phase Diagrams of Ternary Gold Alloys, vol 294, the Institute of Metals, Serie No, 1990.
[26] W.B. Pearson, A Handbook of Lattice Spacing and Structures of Metals and Alloys, Pergamon Press, eBook, 1967, ISBN 9781483226613.
[27] A. Kusoffsky, Thermodynamic evaluation of the ternary Ag-Au-Cu system – including a short range order description, Acta Mater. 50 (2002) 5139–5145, https://doi.org/10.1016/S1359-6454(02)00382-8.
[28] F. Weinberg, Tools and Techniques in Physical Metallurgy, vol 1, Mercel Dekker Inc. N.Y., 1970, 10: 0824717643 ISBN 13: 9780824717643.
[29] R.M. Brick, Structure and Properties of Alloys, Materials Science and Engineering Series, 3 rd edition, Mc Graw Hill Book Co., 1965.
[30] Y.M. Lajtin, in: Mir Moscú (Ed.), Metalografía y Tratamiento Térmico de los Metales, fourth ed., URSS, 1973.
[31] C.R. Brooks, Heat Treatment: Structure and Properties of Nonferrous Alloys, American Society for Metals, 1982, https://doi.org/10.1007/s13632-013-0074-8. ASM International.
[32] R. Wilson, A Practical Approach to Continuous Casting of Copper-Based Alloys and Precious Metals, IOM Communications, London, 2000.
[33] W. Corti Christofer, Metallurgy of micro alloyed 24 carat golds, Gold Bull. 42 (2) (1999) 39–47, https://doi.org/10.1007/BF03214789.